An expanded LUXendin color palette for GLP1R detection and visualization *in vitro* and *in vivo*

Julia Ast[1,2#], Alissa N. Novak[3,#], Tom Podewin[4], Nicholas H.F. Fine[1,2], Ben Jones[5], Alejandra Tomas[6], Ramona Birke[7], Kilian Roßmann[7], Bettina Mathes[4], Jenny Eichhorst[8], Martin Lehmann[8], Amelia K. Linnemann[3,*], David J. Hodson[1,2,*] and Johannes Broichhagen[4,7,*]

[1] Institute of Metabolism and Systems Research (IMSR), and Centre of Membrane Proteins and Receptors (COMPARE), University of Birmingham, Birmingham, UK.
[2] Centre for Endocrinology, Diabetes and Metabolism, Birmingham Health Partners, Birmingham, UK.
[3] Department of Pediatrics, and Indiana Center for Diabetes and Metabolic Diseases, Indiana University School of Medicine, Indianapolis, IN, USA.
[4] Department of Chemical Biology, Max Planck Institute for Medical Research, Heidelberg, Germany.
[5] Imperial College London, Section of Investigative Medicine, Division of Diabetes, Endocrinology and Metabolism, London, UK.
[6] Section of Cell Biology and Functional Genomics, Division of Diabetes, Endocrinology and Metabolism, Imperial College London, London, UK.
[7] Leibniz-Forschungsinstitut für Molekulare Pharmakologie, Berlin, Germany.
[8] Department of Pharmacology and Cell Biology, Leibniz-Forschungsinstitut für Molekulare Pharmakologie, Berlin, Germany.

[#]equal contributions

*Correspondence should be addressed to:
aklinnem@iu.edu, d.hodson@bham.ac.uk, broichhagen@fmp-berlin.de

Keywords: incretin, GLP1R, diabetes, beta cell, fluorescent probes, imaging.

ORCIDs:

Julia Ast: 0000-0002-0039-4762
Alissa N. Novak: 0000-0002-0450-384X
Tom Podewin: 0000-0002-1632-5104
Nicholas H.F. Fine: 0000-0003-2343-8534
Ben Jones: 0000-0003-0461-2584
Alejandra Tomas: 0000-0002-2290-8453
Ramona Birke: n/a
Kilian Roßmann: 0000-0003-4965-9669
Bettina Mathes: n/a
Jenny Eichhorst: n/a
Martin Lehmann: 0000-0002-8370-6353
Amelia K. Linnemann: 0000-0001-7356-4876
David J. Hodson: 0000-0002-8641-8568
Johannes Broichhagen: 0000-0003-3084-6595

ABSTRACT

The glucagon-like peptide-1 receptor (GLP1R) is expressed in peripheral tissues and the brain, where it exerts pleiotropic actions on metabolic and inflammatory processes. Detection and visualization of GLP1R remains challenging, partly due to a lack of validated reagents. Previously, we generated **LUXendins**, antagonistic red and far-red fluorescent probes for specific labeling of GLP1R in live and fixed cells/tissue. We now extend this concept to the green and near-infrared color ranges by synthesizing and testing **LUXendin492**, **LUXendin551**, **LUXendin615** and **LUXendin762**. All four probes brightly and specifically label GLP1R in cells and pancreatic islets. Further, **LUXendin551** acts as chemical beta cell reporter in preclinical rodent models, while **LUXendin762** allows non-invasive imaging, highlighting differentially-accessible GLP1R populations. We thus expand the color palette of **LUXendins** to seven different spectra, opening up a range of experiments using widefield microscopy available in most labs through super-resolution imaging and whole animal imaging. With this, we expect that **LUXendins** will continue to generate novel and specific insight into GLP1R biology.

INTRODUCTION

The glucagon-like peptide-1 receptor (GLP1R) is a class B G protein-coupled receptor involved in the regulation of glucose homeostasis, food intake and inflammation [1]. As such, GLP1R agonist (GLP1RA) therapy has become a mainstay of type 2 diabetes treatment during the past decade, with a number of drugs on the market based upon stabilized analogs of glucagon-like peptide-1 [2]. Most recently, phase III trials of the third generation semaglutide have shown a ~15% reduction in body weight when combined with lifestyle interventions [3], leading to approval of GLP1RA as the first non-surgical treatment for complex obesity. Despite this, information concerning the localization of GLP1R is lacking, primarily due to the paucity of reliable and specific reagents for its detection and visualization [4]. Without this knowledge, it is difficult to elucidate the exact cellular mechanisms underlying GLP1R actions, many of which could be key to developing even more specific or effective treatments for metabolic/inflammatory disease states, by for instance tissue-targeted delivery [5]. For example, GLP1RA have been shown to reduce the progression from non-alcoholic fatty liver disease/non-alcoholic steatohepatitis to fulminant fibrosis [6], yet where and how the GLP1R acts is currently uncertain. Along similar lines, GLP1RA exert inhibitory (and beneficial) effects on glucagon secretion, yet pancreatic GLP1R distribution and signaling remain debated [4]. Lastly, the neural circuits that GLP1RA are able to access to exert effects on food intake remain to be fully delineated [7].

Reagents to detect GLP1R in tissue include antibodies, reporter mice, and fluorescent ligands [4]. Historically, studies with antibodies have been confounded by the use of non-specific antisera, which detect non-GLP1R targets [8]. Two specific antibodies now exist and have been extensively validated, including in GLP1R knockout tissue, or cells heterologously expressing human GLP1R [9]. However, the available antibodies do not perform well for immunofluorescent staining in the brain and cannot be used for live visualization of the GLP1R using microscopy. Reporter mice, where cells that express(ed) GLP1R are selectively labeled with high fidelity, have been used to address this limitation, demonstrating excellent concurrence with other approaches [10]. However, reporter alleles neither visualize the receptor itself nor differentiate cells that once expressed GLP1R, but no longer do so (the cell will be indelibly marked). Fluorescent agonists bind the GLP1R orthosteric site in live tissue and can also be fixed to allow further immunohistochemical analysis [7b, 11]. However, this approach is confounded by activation of GLP1R and as such the unstimulated fraction cannot be studied in live cells.

Most recently, we have developed fluorescent antagonists, which are capable of detecting GLP1R in its unstimulated/antagonized state at the membrane [12]. Advantageously, these probes, termed **LUXendins**, are equipotent to native antagonist, work well in the periphery and brain, display excellent brightness and can be formalin-fixed [12]. To date, **LUXendins** have been freely and widely distributed to dozens of other labs for academic use [13], opening up new GLP1R biology. The **LUXendins** were necessarily furnished with red and far-red fluorophores, not only allowing conventional microscopy, but also for the aims of our study, total internal reflection (TIRF) microscopy and stimulated emission depletion (STED) nanoscopy [12]. Aiming for more experimental modalities and taking on board comments from end users, we now expand the color-palette of the **LUXendins**, further increasing their utility for widefield, confocal, intravital and near-infrared microscopy, allowing imaging from the single cell to the whole animal.

RESULTS

Design and synthesis of LUXendin492, LUXendin551, LUXendin615 and LUXendin762

Exendin4(9-39) was employed as scaffold for modification with fluorophore. Using solid-phase peptide synthesis (SPSS), Exendin4(9-39)-S39C (S39C-Ex4) was generated, bearing a *C*-terminal serine to cysteine substitution for functionalization via the introduced thiol handle. CF488A-, Cy3-, CPY- and Cy7-conjugated versions were produced using cysteine-maleimide reactions and termed **LUXendin492**, **LUXendin551**, **LUXendin615** and **LUXendin762**, respectively (Figure 1A), according to their maximal absorption values. Spectral properties were determined using UV/Vis and fluorescence spectroscopy (Figure 1B and C) (Table 1) and were in line with known properties of the fluorophores used. Full compound characterization and purity assessment are provided in the Supplementary Information.

Table 1: Spectral properties of GLP1R labeling probes. Maximal excitation and emission wavelengths, extinction coefficients, and quantum yields of all **LUXendin** probes.

	dye	λ_{Ex} / nm	λ_{Em} / nm	ε[a] / M^{-1} cm^{-1}	Φ
LUXendin492	CF488A	492	517	70,000[c]	N/A
LUXendin551	Cy3	551	567	150,000[d]	0.31
LUXendin555[b]	TMR	555	579	84,000	0.31
LUXendin615	CPY	615	640	100,000[14]	0.59
LUXendin645[b]	Cy5	645	664	250,000	0.22
LUXendin651[b]	SiR	651	669	100,000	0.43
LUXendin762	Cy7	762	784	199,000[d]	0.30

[a] For maleimide-conjugated fluorophores
[b] previous study
[c] https://biotium.com/technology/cf-dyes/cf488a-dye/
[d] https://de.lumiprobe.com

LUXendin492, LUXendin551, LUXendin615 and LUXendin762 are potent GLP1R antagonists

We first assessed the antagonist activity of the novel **LUXendins** using cAMP assays in SNAP-GLP1R:HEK293 cells. As expected, native GLP1(7-36)NH_2 increased intracellular cAMP levels with a pEC_{50} = 8.3 ± 0.2 (Figure 1D). Application of increasing doses of the benchmark antagonist Exendin4(9-39) inhibited GLP1-stimulated cAMP levels with a pIC_{50} = 7.0 ± 0.2 (Figure 1D). Confirming that the installed fluorophores did not alter potency of the Exendin4(9-39)-S39C backbone, **LUXendin492** (pIC_{50} = 7.2 ± 0.2), **LUXendin551** (pIC_{50} = 7.2 ± 0.1), **LUXendin615** (pIC_{50} = 7.2 ± 0.1) and **LUXendin762** (pIC_{50} = 7.0 ± 0.2) all inhibited GLP1-stimulated (10 nM) cAMP levels in a manner equipotent to Exendin4(9-39) (Figure 1E). The pharmacology of Exendin4(9-39)-S39C has previously been determined [12]. Thus, the novel **LUXendins** show indistinguishable antagonistic properties from Exendin4(9-39) in terms of cAMP signaling. With this in mind, we set out to study novel **LUXendin** labeling in cells and tissues, as well as the whole organism.

LUXendin492, LUXendin551 and LUXendin615 specifically label GLP1R

To establish the labeling efficacy and specificity of the novel **LUXendins**, SNAP-GLP1R:CHO-K1 cells were incubated with each probe, before washing and orthogonal SNAP labeling with cell impermeable SBG-TMR or SBG-SiR [15]. High-resolution confocal images showed predominantly membrane-localized **LUXendin** staining in SNAP-GLP1R:CHO-K1 cells, which overlapped with labeling of the SNAP-tag located on the GLP1R *N*-terminus (Figure 2A). No signal was detected in mock (non-transfected) CHO-K1 cell controls (Supplementary Figure S1). **LUXendins** were also able to label stably-transfected SNAP_GLP1R:INS1 832/3 rat beta cells (Figure 2B), as well as native INS1 832/3, which endogenously express GLP1R (Figure 2C). Demonstrating high specificity, signal was absent in INS1 832/3 GL1PR$^{-/-}$ cells, CRISPR deleted for the GL1PR (Figure 2B, C). Of note, **LUXendin492** and **LUXendin615** staining was less 'clean' than **LUXendin551**, with some fluorescent signal present in the cytoplasm. We have previously reported a similar staining distribution for **LUXendin555** (TMR) versus **LUXendin645** (Cy5) [12], demonstrating a general preference toward cyanine-based dyes over their xanthene-based counterparts for cell labeling. Nonetheless, all the **LUXendins** tested clearly label membrane **GLP1R**. We next validated the **LUXendins** for use in widefield microscopy, which is widely available in most labs, serves to illustrate the robustness of labeling, and has the added advantage of allowing detection of near-infrared probes using cost efficient and fast switchable LED excitation and sensitive sCMOS detectors. As for confocal imaging, a similar pattern of **LUXendin492**, **LUXendin551**, **LUXendin615** staining was seen, with the cyanine-based dye (LUX551) performing superiorly (Supplementary Figure 2).

LUXendin492, LUXendin551 and LUXendin615 specifically label endogenous GLP1R

One of the major advantages of **LUXendins** is that they can be used to visualize GLP1R in both live and fixed complex tissues. Pancreatic islets of Langerhans served as the testbed for the novel **LUXendins**, since they express GLP1R, which is predominantly localized to the beta cell compartment [4, 12]. Following one hour incubation with **LUXendin492**, **LUXendin551** and **LUXendin615**, intense labeling was observed throughout the islet, with large gaps apparent (presumably representing the GLP1R-negative alpha cell compartment, which comprises ~20% of the rodent islet, as reported [12]) (Figure 3A). In all cases, labeling with the novel **LUXendins** could still be observed following formalin-fixation (Figure 3B), further expanding the utility of the novel **LUXendins** for protein identification together with immunohistochemistry. Confirming specificity, **LUXendin492, LUXendin551** and **LUXendin615** signals co-localized with specific GLP1R monoclonal antibody staining (Novo Nordisk 7F38, fully validated in GLP1R$^{-/-}$ tissue [12]) (Figure 3B).

LUXendin551 allows in vivo fluorescent labeling of islets in NOD mice

The NOD mouse is a type 1 diabetes model that develops insulitis at 4-8 weeks of age, with frank diabetes occurring from 30 weeks of age [16]. However, identifying beta cells during disease trajectory is challenging, since the polygenic NOD genetic background cannot easily be recombined with common inbred beta cell reporter strains (e.g. Ins1Cre;R26YFP). We and others have previously shown that GLP1R expression is beta cell specific [10b, 12] and we thus hypothesized that **LUXendins** might open up the possibility to identify beta cells in NOD (and other polygenic) mice.

To investigate this, the pancreas was exposed in 8-week-old anesthetized NOD mice through a small abdominal incision, before being subjected to two-photon microscopy (Figure 4A).

Baseline images were acquired following retro-orbital injection of Hoechst33342 and albumin-AF647 to label the nuclei and vasculature, respectively. Prior to **LUXendin551** injection there was no detectable signal (Figure 4B). Rapid labeling occurred following the administration of **LUXendin551** and was detected for at least 30 min post-injection (Figure 4B). These studies also demonstrated **LUXendin551** is highly specific to islets and provides the ability to distinguish islets and beta cells from exocrine tissue (Figure 4C).

LUXendin762 allows non-invasive fluorescent detection of GLP1R in vivo

Due to its near-infrared excitation, we surmised that a Cy7-based dye, **LUXendin762**, might allow intravital labeling of GLP1R, visible using the widely available and non-invasive IVIS in vivo imaging systems. We first tested **LUXendin762** in cellulo in SNAP-GLP1R:CHO-K1 cells and in keeping with its pharmacology were able to detect strong membrane-labelling, with little evidence of intracellular accumulation, again pointing to the high performance of cyanine-based dyes (Figure 5A). **LUXendin762** was next used to label primary islets, again showing cell-membrane localization (Supplementary Figure 3A), shown to be GLP1R-positive using validated monoclonal antibody (Supplementary Figure 3B). No spectral overlap could be detected between Cy5 (**LUXendin645**) and Cy7 (**LUXendin762**) channels (Supplementary Figure 3A, B).

Confident that **LUXendin762** was able to specifically label GLP1R, we next injected Nude mice with the probe before imaging. Strong fluorescent signal could be detected in the abdomen and brain at 30 min and 60 min following intraperitoneal or subcutaneous injection, with fluorescence levels ~2-5-fold higher than in animals receiving saline vehicle (Figure 5B). Harvest of various organs showed the highest fluorescent signal in the pancreas of mice receiving intraperitoneal **LUXendin762**, with brain, lung, kidney and heart being similar to saline-treated controls (Figure 5C). By contrast, mice receiving subcutaneous **LUXendin762** displayed the highest probe levels in the brain, whereas no signal was detected in the pancreas, lung, kidney and heart versus saline-treated control (Figure 5D). Notably, the brain and pancreas are known to be GLP1R-positive [4], whereas protein expression of the receptor in the lung, kidney and heart is in small cell populations (e.g. smooth muscle of arterioles) or absent [9b, 17]. Together, these studies show that **LUXendin762** signal can be detected in vivo in the whole organism, and reveal a novel role for injection route in determining GLP1R access.

DISCUSSION

In the present study, we synthesize and validate **LUXendin492**, **LUXendin551**, **LUXendin615** and **LUXendin762**, antagonist probes spanning green to near infrared for the visualization of GLP1R in cells, tissues and animals. Together with our previous **LUXendin555**, **LUXendin645** and **LUXendin651** probes [12], we now extend the **LUXendin** color palette to seven different spectra. These probes contain a range of different fluorophores suitable for widefield, confocal, super-resolution and intravital imaging, as well as FACS.

Pharmacologically, the novel **LUXendins** behave as full antagonists at the GLP1R, with similar potency to benchmark Exendin4(9-39). These studies further validate the robustness of the synthetic approach used and highlight the advantages of the S39C *C*-terminally substituted backbone used previously for Exendin4(9-39) [12] and Exendin4(1-39) [18]. We envisage that a similar backbone might in the future be amenable to functionalization with biotin, complexed lanthanides, singlet oxygen generators or even nanogold particles, for example to allow non-fluorescent labeling for mass spectrometry, magnetic resonance imaging or electron microscopy. With our observation that cyanine fluorophores behave more 'cleanly' in microscopic experiments, we are eager to find out how other molecular markers and tracers behave, and these endeavours are of ongoing interest in our laboratories.

Of note, labeling with the novel **LUXendins** was co-localized with both SNAP-GLP1R and specific monoclonal antibody staining, as expected given the previous thorough validation of **LUXendin555**, **LUXendin645** and **LUXendin651** stablemates [12]. Moreover, no LUXendin signal could be detected in INS1 832/3 cells CRISPR-deleted for the GLP1R. These data also confirm that the Exendin4-S39C scaffold tolerates a range of fluorophores without significant effects on labeling or pharmacology. While some punctate staining was seen with non-cyanine dyes, this might reflect cleavage of fluorophore rather than GLP1R activation, since: 1) all **LUXendins** were potent antagonists; 2) no co-localization from intracellular signals were seen in SNAP-GLP1R cell systems; and 3) we previously showed that punctate **LUXendin** signal was not co-localized with GLP1R monoclonal antibody [12]. We observed pronounced increases in performance of cyanine dyes (Cy3, Cy5 and Cy7) when compared to CF488, TMR, and CPY, most probably due to their molecular nature. Lastly, we omitted functionalization with Alexa Fluors, since previous efforts directed at SNAP-GLP1R did not lead to appreciable labeling, presumably because the presence of multiple negatively-charged sulfonate moieties interfere with target binding.

Using novel **LUXendins**, we were able to perform unprecedented experiments and reveal new biology regarding GLP1R. As the best performing dye, **LUXendin551** allowed GLP1R and thus beta cells to be reported in intravital experiments of a type 1 diabetes preclinical mouse model, which is not amenable to further genetic manipulation. Such experiments are important, since we are still lacking information on the changes that occur in beta cell mass (and GLP1R expression) during the insulitis and autoimmune destruction [19]. To allow non-invasive imaging, Cy7 was installed on the **LUXendin** backbone to produce **LUXendin762**, a near-infrared probe. We were able to demonstrate that **LUXendin762** signal can be recorded in vivo (compared to saline-treated controls) and sequesters in organs known to express the GLP1R such as the pancreas and brain [4]. Of interest, **LUXendin762** highlighted differential access routes to peripheral and brain GLP1R sites, with subcutaneous and not intraperitoneal injection labelling the latter. While the mechanisms are currently unknown, we speculate that ligand injected subcutaneously is less prone to the first pass effect and as such is able to

abundantly enter the carotid arteries for entry into the brain. **LUXendin762** thus opens up for the first time non-invasive longitudinal studies of GLP1R in mice using readily accessible platforms available in most academic/industrial animal facilities. Such studies are particularly pertinent, since GLP1R is also a readout for beta cell mass in preclinical models of type 2 diabetes and other metabolic syndromes [20]. Furthermore, longitudinal measures in the same animal are statistically more powerful and refined compared to assessment of various timepoints in multiple cohorts.

In summary, a total of seven **LUXendins** now allow detection and labelling of GLP1R in five different colors, with fluorophores tailored for various imaging modalities. We anticipate that these specific and validated probes will provide further insight into GLP1R biology in the periphery and brain, with implications for treatment with GLP1RA.

METHODS

Synthesis

Exendin4(9-39)-S39C was generated as previously reported using solid phase peptide synthesis[12, 18]. TSTU activation of CPY-6-COOH and reaction with 1-(2-amino-ethyl)-pyrrole-2,5-dione (TFA salt, Aldrich) yielded Mal-CPY. Maleimide conjugated CF488A (Aldrich), Cy3, and Cy7 (both Lumiprobe) were purchased from commercial vendors. Coupling to peptides was performed using thiol-maleimide chemistry in PBS, before characterization of novel compounds using HRMS and purity (>95%) measurement using HPLC. Extinction coefficients and quantum yields were based upon available manufacturer measures for CF488-Mal, Cy3-Mal, CPY-6-COOH and Cy7-Mal. Details for synthesis including characterization of **LUXendin492**, **LUXendin551**, **LUXendin615** and **LUXendin762** are provided in the Supporting Information.

Cell culture

CHO-K1 cells stably expressing the human SNAP-GLP1R (Cisbio) (SNAP-GLP1R:CHO-K1) were maintained at 5% CO_2, 37 °C in high-glucose phenol red Glutamax containing DMEM (Invitrogen, 31966047) supplemented with 10% heat-inactivated FCS (Invitrogen), 1% penicillin/streptomycin (Invitrogen), 500 µg/mL G418 (Invitrogen), 25 mM HEPES (Invitrogen) and 1% nonessential amino acids (Invitrogen), or DMEM (D6546, Sigma) supplemented with 10% FBS (Merck), 1% penicillin/streptomycin (Fisher Scientific), 500 µg/mL G418 (Fisher Scientific), 25 mM HEPES (Merck), 1% non-essential amino acids (Merck) and 2% L-glutamine (Thermo Scientific). The same medium without G418 was used to culture CHO-K1 cells. HEK293:SNAP-GLP1R cells were cultured in DMEM supplemented with 10% FBS, 1% penicillin/streptomycin and 1 mg/ml G418. INS1 832/3 wt and GLP1R$^{-/-}$ cells [21] were cultured in RPMI supplemented with 11 mM glucose, 10% FCS, 10 mM HEPES, 2 mM L-glutamine, 1 mM pyruvate, 50 µM β-mercaptoethanol and 1% penicillin/streptomycin and maintained as above. SNAP-GLP1R:INS1 832/3 cells were cultured as INS1 832/3 wt with the addition of 500 µg/mL G418.

Animals

All studies with harvested tissue used 7–10 week-old male C57BL6/J mice, and were regulated by the Animals (Scientific Procedures) Act 1986 of the U.K (Personal Project Licenses P2ABC3A83 and PP1778740). Approval was granted by the University of Birmingham's Animal Welfare and Ethical Review Body. All in vivo imaging experiments were performed with approval and oversight from the Indiana University Institutional Animal Care and Use Committee (IACUC).

Islet isolation

Animals were humanely euthanized using cervical dislocation, before injection of collagenase 1 mg/mL (Serva NB8) into the bile duct. Inflated pancreases were digested for 12 min at 37 °C and islets separated using a Ficoll (Sigma-Aldrich) gradient. Islets were cultured in RPMI medium containing 10% FCS, 100 units/mL penicillin, and 100 µg/mL streptomycin.

cAMP assays

cAMP assays were performed in SNAP-GLP1R:HEK293 cells, as previously described.[18] Briefly, cells were incubated with 10 nM GLP-1(7-36)NH_2 alongside increasing concentrations of **LUXendin** for 30 min, before lysis and measurement of cAMP using a HTRF (Cisbio) assay, according to the manufacturer's instructions. All assays were performed in the presence of 100-500 µM IBMX to inhibit phosphodiesterase activity. pEC_{50} and pIC_{50} values were calculated using log concentration-response curves fitted with a three- or four-parameter equation.

Live imaging

CHO-K1 and SNAP-GLP1R:CHO-K1 cells were seeded (60,000 cells/well) on µ-slide 8-well glass bottom dishes (ibidi, 80826) and grown for 2 days at 37 °C in a humidified 5% CO_2 incubator. For imaging, cells were incubated for 30 min at 37 °C in a humidified 5% CO_2 incubator in culture medium supplemented with 200 nM **LUXendin** and 5 µM Hoechst33342. Cells were washed once in cell culture medium and imaged in live cell imaging buffer (Invitrogen, A14291DJ) at 37 °C and 5% CO_2 using a Ti-E Nikon epifluorescence microscope equipped with pE4000 (cool LED), Penta Cube (AHF 66-615), 60x oil NA 1.49 (Apo TIRF Nikon) and imaged on SCMOS camera (Prime 95B, Photometrics) operated by NIS Elements (Nikon). For excitation the following wavelengths were used: **LUXendin492**: λ = 470 nm; **LUXendin551**: λ = 550 nm; **LUXendin615**: λ = 595 nm; **LUXendin645**: λ = 635 nm; **LUXendin762**: λ = 740 nm.

For confocal imaging, CHO-K1 and SNAP-GLP1R:CHO-K1 were seeded in 96-well glass-bottom plates (Eppendorf, E0030741030) and kept at 37 °C and 5% CO_2 until labeling in culture media supplemented with 200 nM **LUXendin** and 500 nM SNAP label at 37 °C, 5% CO_2 for 30 min and 4.4 µM Hoechst33342 for 5 min. After one wash cells were imaged in culture media using an LSM880 meta-confocal microscope equipped with GaAsP spectral detectors and a 63x water NA 1.20 objective. For excitation / emission the following wavelengths were used: Hoechst33324: λ = 405 nm / 410-507 nm, **LUXendin492**: λ = 488 nm / 490-560 nm, **LUXendin551** and SBG-TMR: λ = 561 nm / 570-622 nm, **LUXendin615** and SBG-SiR: λ = 633 nm / 638-759 nm.

INS1 832/3, INS1 832/3 $GLP1R^{-/-}$ and SNAP-GLP1R:INS1 832/3 cells were plated onto Mattek glass bottom dishes the day before imaging, and imaged on a Zeiss LMS780 confocal microscope using a Plan-Apochromat 63x oil 1.40 NA objective for 2 min after addition of 100 nM LUXendin.

Islets were incubated with 100 nM **LUXendin492**, **LUXendin551** or **LUXendin615** for 1 h at 37 °C in culture medium. Islets were washed three times and were imaged in culture medium using a Zeiss LSM880 AxioObserver microscope equipped with GaAsP spectral detectors and a 40x water NA 1.2 Korr FCS M27 objective. For excitation / emission the following wavelengths were used: **LUXendin492**: λ = 488 nm / 498-569 nm. **LUXendin551**: λ = 561 nm / 569-667 nm. **LUXendin615**: λ = 633 / 641-694 nm.

Immunostaining

Islets were incubated with 100 nM **LUXendin492**, **LUXendin551, LUXendin615** and **LUXendin762** for 1 h at 37 °C in culture medium, before 4% formaldehyde fixation for 10 min. Mouse monoclonal anti-GLP1R 1:30 (Iowa DHSB; mAb #7F38) was applied overnight at 4 °C in PBS + 0.1% Triton + 1% BSA. Secondary antibodies were applied for 1 h at room

temperature and included goat anti-mouse DyLight488 (excitation λ = 488 nm, emission λ = 489-552 nm) and goat anti-mouse Alexa Fluor 633 (excitation λ = 633 nm, emission λ = 641-694 nm). Samples were mounted on slides using Vectashield Hardset containing DAPI. Imaging was performed using a Zeiss LSM880 AxioObserver microscope, as above, for **LUXendin492**, **LUXendin551, LUXendin615**, and using a TIE Nikon epifluorescence microscope, as above, for **LUXendin762**.

Two Photon *in vivo* Imaging

Female NOD/ShiLtJ mice 8 weeks of age were anesthetized with isoflurane. A small, vertical incision was made to expose the intact pancreas. Then, the exposed pancreas was placed on a 50 mm glass-bottom dish for imaging on an inverted microscope. Body temperature was maintained using heating pads and heating elements on the objective. The mouse received, via retro-orbital injection, Hoechst 33342 (1 mg/kg in PBS) to label nuclei, albumin-AF647 (1 mg/kg in PBS) to label vasculature, and 75 µL of 30 µM **LUXendin551**. Images were collected using a Leica SP8 microscope, equipped with a ×25/0.95 NA objective and Spectra Physics MaiTai DeepSee mulitphoton laser. Excitation was delivered at λ = 800 nm for Hoechst and Albumin-AF647, with signals collected at λ = 410-500 nm and λ = 550-590 nm, respectively. **LUXendin551** was excited at λ = 1050, with signal collected at 650-700 nm. A conventional PMT was used for Hoechst, with a HyD detector used for Albumin-AF647 and **LUXendin551**. Blood was collected from the tail vein prior to and 30 min after **LUXendin555** injection, and glucose was measured using an AlphaTrak2 glucometer. After imaging, unconscious mice are euthanized by cervical dislocation.

Non-invasive *in vivo* imaging

Whole body fluorescence accumulation and distribution was assessed in male athymic nude mice 8 weeks of age using an IVIS Spectral CT (Perkin Elmer). Mice were anesthetized with inhaled isoflurane and baseline images were acquired. Then, mice were intraperitoneally or subcutaneously injected with 100 µL of saline or 5 µM **LUXendin762**. Images were collected using a broad excitation and emission series combination ranging from 640 to 675 nm and 680 to 760 nm, respectively at 30 minutes and 1 hour post injection. At the end point, animals were sacrificed, and tissues (pancreas, heart, brain, lung, kidney, liver, and spleen) were harvested for *ex vivo* fluorescent analysis. Spectral unmixing and quantification were analyzed using Living Image Software.

REFERENCES

[1] a) J. E. Campbell, D. J. Drucker, *Cell Metab* **2013**, *17*, 819-837; b) D. J. Drucker, *Cell Metabolism* **2018**, *27*, 740-756.

[2] J. M. Trujillo, W. Nuffer, B. A. Smith, *Therapeutic Advances in Endocrinology and Metabolism* **2021**, *12*.

[3] J. P. H. Wilding, R. L. Batterham, S. Calanna, M. Davies, L. F. Van Gaal, I. Lingvay, B. M. McGowan, J. Rosenstock, M. T. D. Tran, T. A. Wadden, S. Wharton, K. Yokote, N. Zeuthen, R. F. Kushner, S. S. Group, *N Engl J Med* **2021**, *384*, 989.

[4] B. A. McLean, C. K. Wong, J. E. Campbell, D. J. Hodson, S. Trapp, D. J. Drucker, *Endocrine Reviews* **2020**.

[5] C. Ammala, W. J. Drury, 3rd, L. Knerr, I. Ahlstedt, P. Stillemark-Billton, C. Wennberg-Huldt, E. M. Andersson, E. Valeur, R. Jansson-Lofmark, D. Janzen, L. Sundstrom, J. Meuller, J. Claesson, P. Andersson, C. Johansson, R. G. Lee, T. P. Prakash, P. P. Seth, B. P. Monia, S. Andersson, *Sci Adv* **2018**, *4*, eaat3386.

[6] a) M. J. Armstrong, P. Gaunt, G. P. Aithal, D. Barton, D. Hull, R. Parker, J. M. Hazlehurst, K. Guo, G. Abouda, M. A. Aldersley, D. Stocken, S. C. Gough, J. W. Tomlinson, R. M. Brown, S. G. Hübscher, P. N. Newsome, *The Lancet* **2016**, *387*, 679-690; b) P. N. Newsome, K. Buchholtz, K. Cusi, M. Linder, T. Okanoue, V. Ratziu, A. J. Sanyal, A.-S. Sejling, S. A. Harrison, *New England Journal of Medicine* **2021**, *384*, 1113-1124.

[7] a) D. I. Brierley, M. K. Holt, A. Singh, A. de Araujo, M. McDougle, M. Vergara, M. H. Afaghani, S. J. Lee, K. Scott, C. Maske, W. Langhans, E. Krause, A. de Kloet, F. M. Gribble, F. Reimann, L. Rinaman, G. de Lartigue, S. Trapp, *Nature Metabolism* **2021**, *3*, 258-273; b) A. Secher, J. Jelsing, A. F. Baquero, J. Hecksher-Sorensen, M. A. Cowley, L. S. Dalboge, G. Hansen, K. L. Grove, C. Pyke, K. Raun, L. Schaffer, M. Tang-Christensen, S. Verma, B. M. Witgen, N. Vrang, L. Bjerre Knudsen, *Journal of Clinical Investigation* **2014**, *124*, 4473-4488; c) S. Gabery, C. G. Salinas, S. J. Paulsen, J. Ahnfelt-Rønne, T. Alanentalo, A. F. Baquero, S. T. Buckley, E. Farkas, C. Fekete, K. S. Frederiksen, H. C. C. Helms, J. F. Jeppesen, L. M. John, C. Pyke, J. Nøhr, T. T. Lu, J. Polex-Wolf, V. Prevot, K. Raun, L. Simonsen, G. Sun, A. Szilvásy-Szabó, H. Willenbrock, A. Secher, L. B. Knudsen, *JCI Insight* **2020**, *5*.

[8] a) N. Panjwani, E. E. Mulvihill, C. Longuet, B. Yusta, J. E. Campbell, T. J. Brown, C. Streutker, D. Holland, X. Cao, L. L. Baggio, D. J. Drucker, *Endocrinology* **2013**, *154*, 127-139; b) C. Pyke, L. B. Knudsen, *Endocrinology* **2013**, *154*, 4-8.

[9] a) C. B. Jensen, C. Pyke, M. G. Rasch, A. B. Dahl, L. B. Knudsen, A. Secher, *Endocrinology* **2018**, *159*, 665-675; b) C. Pyke, R. S. Heller, R. K. Kirk, C. Orskov, S. Reedtz-Runge, P. Kaastrup, A. Hvelplund, L. Bardram, D. Calatayud, L. B. Knudsen, *Endocrinology* **2014**, *155*, 1280-1290.

[10] a) P. Richards, H. E. Parker, A. E. Adriaenssens, J. M. Hodgson, S. C. Cork, S. Trapp, F. M. Gribble, F. Reimann, *Diabetes* **2013**, *63*, 1224-1233; b) S. M. Gray, Y. Xin, E. C. Ross, B. M. Chazotte, M. E. Capozzi, K. El, B. Svendsen, P. Ravn, K. W. Sloop, J. Tong, J. Gromada, J. E. Campbell, D. A. D'Alessio, *J Biol Chem* **2020**.

[11] a) S. M. Clardy, E. J. Keliher, J. F. Mohan, M. Sebas, C. Benoist, D. Mathis, R. Weissleder, *Bioconjugate Chemistry* **2013**, *25*, 171-177; b) J. Lehtonen, L. Schäffer, M. G. Rasch, J. Hecksher-Sørensen, J. Ahnfelt-Rønne, *Islets* **2016**, *7*, e1137415.

[12] J. Ast, A. Arvaniti, N. H. F. Fine, D. Nasteska, F. B. Ashford, Z. Stamataki, Z. Koszegi, A. Bacon, B. J. Jones, M. A. Lucey, S. Sasaki, D. I. Brierley, B. Hastoy, A. Tomas, G. D'Agostino, F. Reimann, F. C. Lynn, C. A. Reissaus, A. K. Linnemann, E. D'Este, D. Calebiro, S. Trapp, K. Johnsson, T. Podewin, J. Broichhagen, D. J. Hodson, *Nature Communications* **2020**, *11*.

[13] a) Z. Fang, S. Chen, Y. Manchanda, S. Bitsi, P. Pickford, A. David, M. M. Shchepinova, I. R. Corrêa Jr, D. J. Hodson, J. Broichhagen, E. W. Tate, F. Reimann, V. Salem, G. A. Rutter, T. Tan, S. R. Bloom, A. Tomas, B. Jones, *International Journal of Molecular Sciences* **2020**, *21*; b) P. Pickford, M. Lucey, Z. Fang, S. Bitsi, J. B. Serna, J. Broichhagen, D. J. Hodson, J. Minnion, G. A. Rutter, S. R. Bloom, A. Tomas, B. Jones,

British Journal of Pharmacology **2020**, *177*, 3905-3923; c) Z. Fang, S. Chen, P. Pickford, J. Broichhagen, D. J. Hodson, I. R. Corrêa, S. Kumar, F. Görlitz, C. Dunsby, P. M. W. French, G. A. Rutter, T. Tan, S. R. Bloom, A. Tomas, B. Jones, *ACS Pharmacology & Translational Science* **2020**, *3*, 345-360.

[14] A. N. Butkevich, G. Y. Mitronova, S. C. Sidenstein, J. L. Klocke, D. Kamin, D. N. H. Meineke, E. D'Este, P.-T. Kraemer, J. G. Danzl, V. N. Belov, S. W. Hell, *Angewandte Chemie International Edition* **2016**, *55*, 3290-3294.

[15] P. Poc, V. A. Gutzeit, J. Ast, J. Lee, B. J. Jones, E. D'Este, B. Mathes, M. Lehmann, D. J. Hodson, J. Levitz, J. Broichhagen, *Chemical Science* **2020**, *11*, 7871-7883.

[16] A. J. King, *Br J Pharmacol* **2012**, *166*, 877-894.

[17] L. L. Baggio, B. Yusta, E. E. Mulvihill, X. Cao, C. J. Streutker, J. Butany, T. P. Cappola, K. B. Margulies, D. J. Drucker, *Endocrinology* **2018**, *159*, 1570-1584.

[18] T. Podewin, J. Ast, J. Broichhagen, N. H. F. Fine, D. Nasteska, P. Leippe, M. Gailer, T. Buenaventura, N. Kanda, B. J. Jones, C. M'Kadmi, J.-L. Baneres, J. Marie, A. Tomas, D. Trauner, A. Hoffmann-Röder, D. J. Hodson, *ACS Central Science* **2018**, *4*, 166-179.

[19] B. O. Roep, S. Thomaidou, R. van Tienhoven, A. Zaldumbide, *Nat Rev Endocrinol* **2021**, *17*, 150-161.

[20] N.-Y. Kang, A. A. P. Soetedjo, N. S. Amirruddin, Y.-T. Chang, O. Eriksson, A. K. K. Teo, *Trends in Molecular Medicine* **2019**, *25*, 708-722.

[21] J. Naylor, A. T. Suckow, A. Seth, D. J. Baker, I. Sermadiras, P. Ravn, R. Howes, J. Li, M. R. Snaith, M. P. Coghlan, D. C. Hornigold, *Biochem J* **2016**, *473*, 2881-2891.

ACKNOWLEDGMENTS

D.J.H. was supported by a Diabetes UK R.D. Lawrence (12/0004431) Fellowship, a Wellcome Trust Institutional Support Award, MRC Confidence in Concept, MRC (MR/N00275X/1 and MR/S025618/1) Project and Diabetes UK (17/0005681) Project Grants. A.T. and B.J. were funded by an MRC Project Grant (MR/R010676/1). A.K.L. was supported by R03 DK115990 (to A.K.L.) and Human Islet Research Network UC4 DK104162 (to A.K.L.; RRID:SCR_014393), and R01DK124380 (to A.K.L.). Intravital microscopy core services were supported by NIH NIDDK Grant P30 DK097512 to the Indiana University School of Medicine. This project has received funding from the European Research Council (ERC) under the European Union's Horizon 2020 research and innovation programme (Starting Grant 715884 to D.J.H.). B.J. is supported by an Imperial post-doctoral, post-CCT research fellowship (IPPRF), the Academy of Medical Sciences, Society for Endocrinology, The British Society for Neuroendocrinology, the European Federation for the Study of Diabetes, and an EPSRC capital award. A.T. also acknowledges funding from Diabetes UK, the European Federation for the Study of Diabetes and the Commonwealth. We are grateful to Kai Johnsson (MPIMR) for support, Ines Kretzschmar and Rudolf Volkmer (both FMP) for peptide synthesis, the Nazare group for analysis (FMP) and Fan Liu (FMP) for mass spectrometry.

CONTRIBUTIONS

D.J.H. and J.B. devised the studies. J.A., A.N.N., N.H.F.F., T.P., B.J., A.T., R.B., K.R., B.M., J.E., A.K.L., D.J.H. and J.B. performed experiments and analyzed data. B.J. provided cell lines. M.L., A.K.L., D.J.H. and J.B. supervised the work. D.J.H. and J.B. wrote the manuscript with input from all the authors.

COMPETING INTERESTS

The authors declare no conflict of interest.

FIGURES

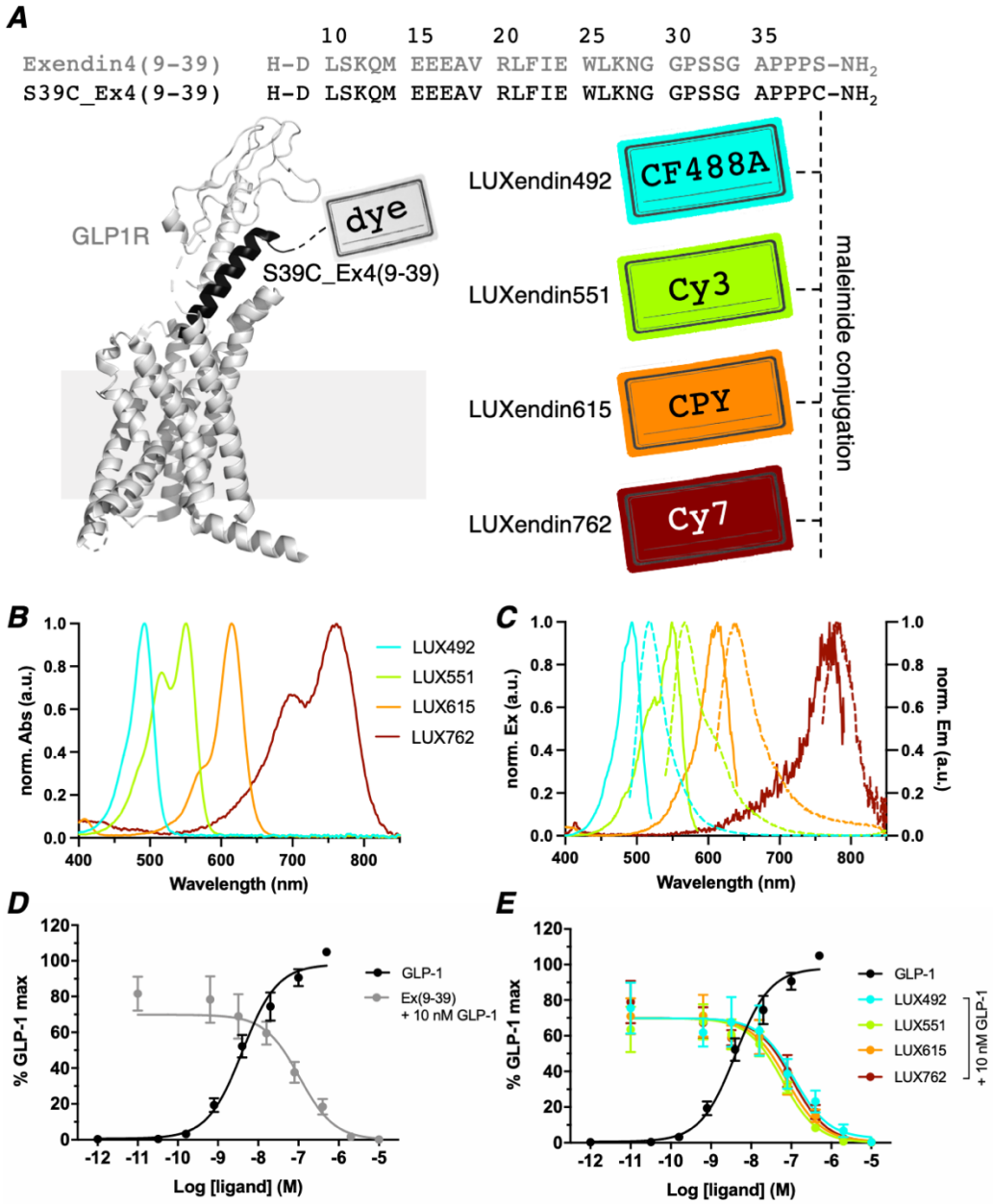

Figure 1: Sequence, structure, photophysical properties and pharmacology of LUXendin492, LUXendin551, LUXendin615 and LUXendin762. A) LUXendins are based on the antagonist Exendin4(9-39) with a S39C mutation to install fluorophores via late-stage thiol-maleimide chemistry. The model shows GLP1R in complex with a peptide ligand (pdb: 5VAI, cartoon obtained by the in-built building capability of PyMOL (Palo Alto, CA, USA)). CF488A, Cy3, CPY or Cy7 were installed as fluorescent labels to give **LUXendin492, LUXendin551, LUXendin615** and **LUXendin762**, respectively. **B)** UV/Vis spectra of the novel **LUXendins**. **C)** Fluorescent excitation and emission spectra of **LUXendins**. **D)** cAMP response in GLP1R-transfected HEK293 cells for GLP-1 (agonist, black) and Ex(9-39) (antagonist) in the presence of 10 nM GLP-1 (gray) (n = 6 independent repeats). **E)** As for **D)**, but in response to **LUXendins**, showing the antagonistic nature of the probes.

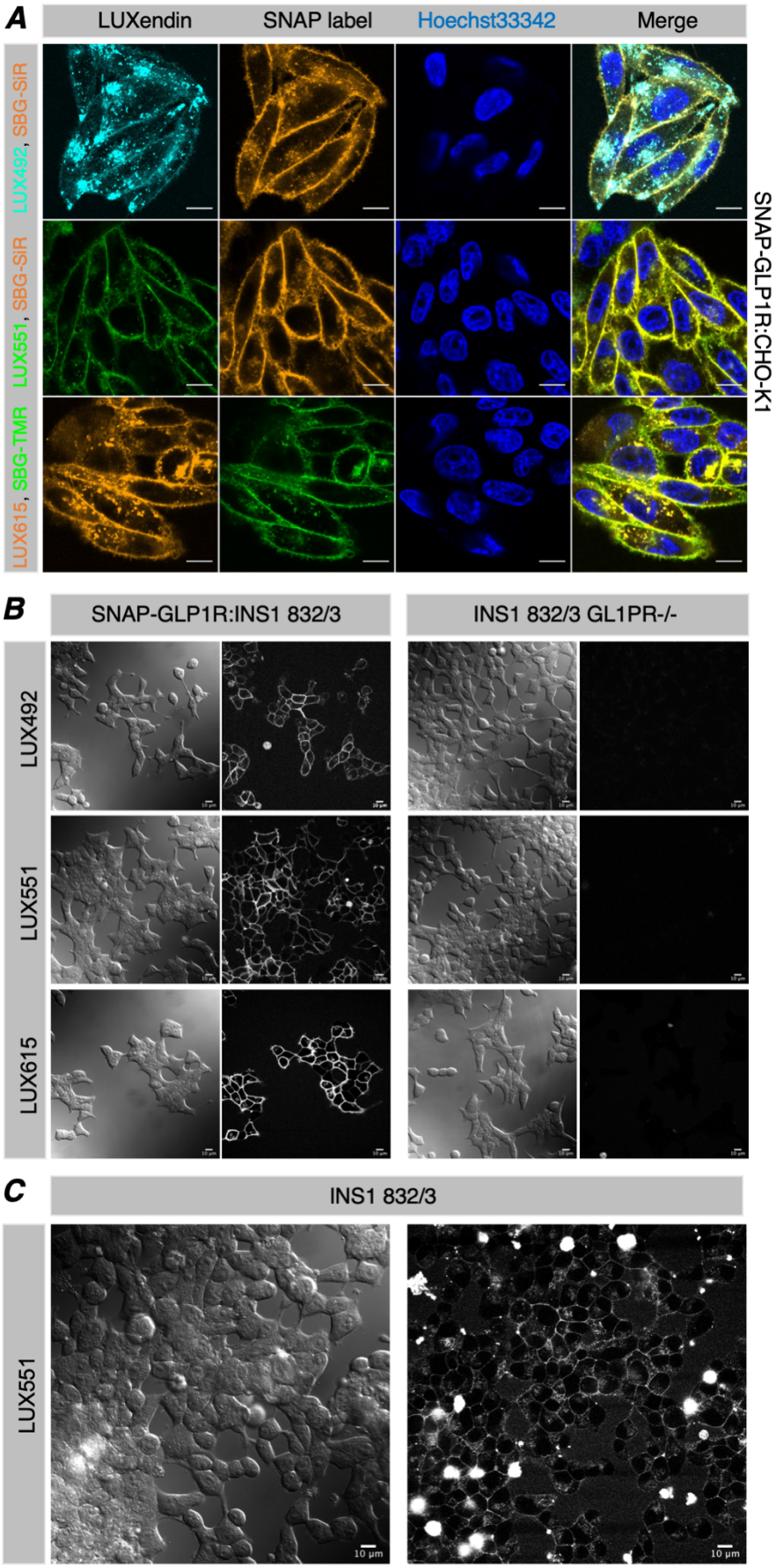
A
LUXendin
SNAP label
Hoechst33342
Merge
LUX492, SBG-SiR
LUX551, SBG-SiR
LUX615, SBG-TMR
SNAP-GLP1R:CHO-K1
B
SNAP-GLP1R:INS1 832/3
INS1 832/3 GL1PR-/-
LUX492
LUX551
LUX615
C
INS1 832/3
LUX551
10 µm
10 µm

Figure 2: A) Labelling of live cells with LUXendin492, LUXendin551 and LUXendin615. SNAP-GLP1R:CHO-K1 were incubated with **LUXendin492** (LUX492), **LUXendin551** (LUX551) and **LUXendin615** (LUX615), before orthogonal SNAP-labelling with either cell impermeable SBG-TMR or SBG-SiR and confocal imaging (nuclei were stained using Hoechst33342) (scale bar = 10 µm) (n = three images from experiments performed in duplicate). **B) LUXendin492, LUXendin551** and **LUXendin615** label SNAP-GLP1R:INS1 832/3, but not INS1 832/3 GLP1R$^{-/-}$ cells. **C)** Additionally, endogenous GLP1R, which is expressed at lower levels than in islets, can be visualized with **LUXendin551 in** INS1 832/3 cells (scale bars = 10 µm).

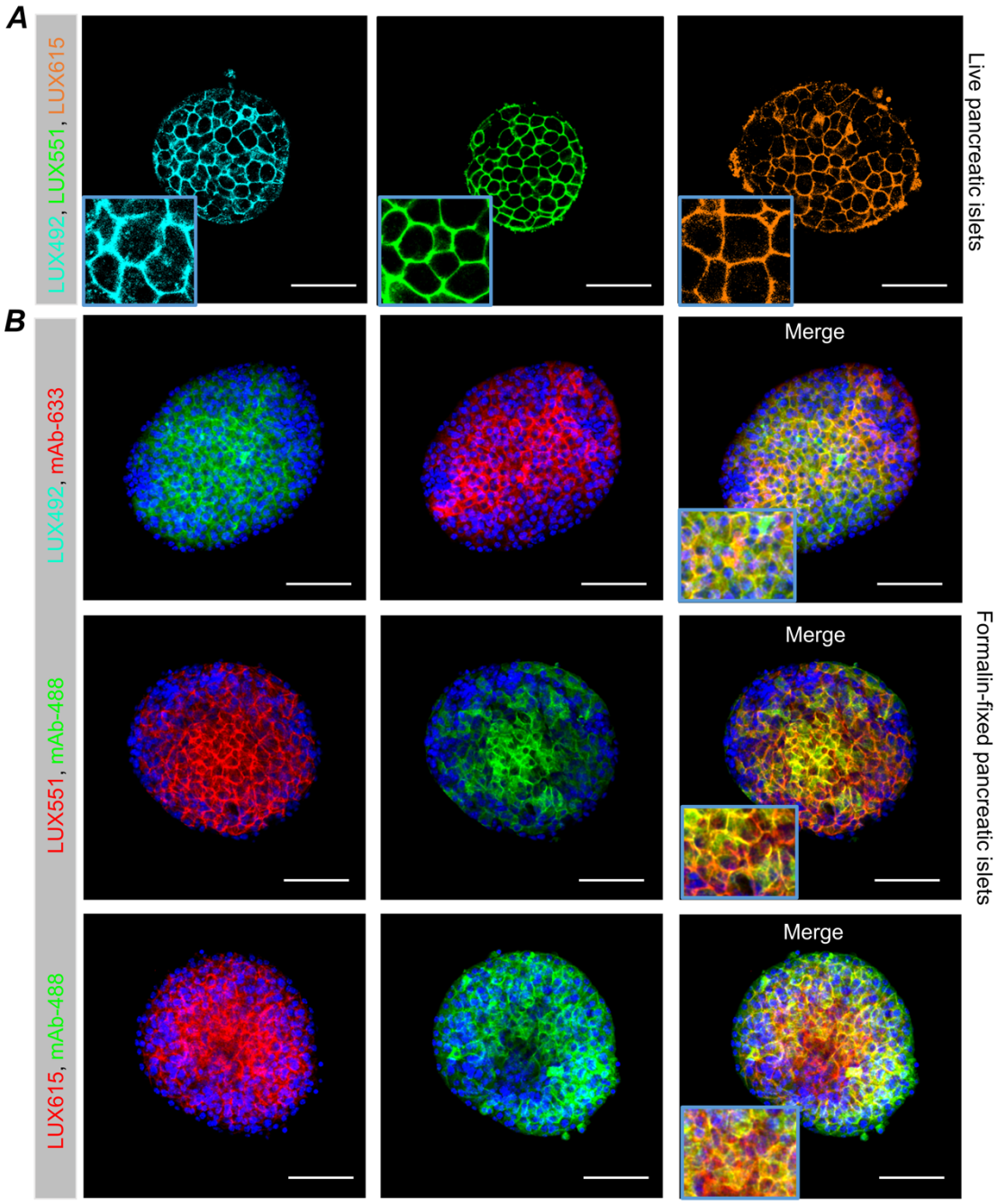

Figure 3: Labelling of live and fixed islets of Langerhans with LUXendin492, LUXendin551 and LUXendin615. A) Incubation of live islets with **LUXendin492** (LUX492), **LUXendin551** (LUX551), or **LUXendin615** (LUX615) leads to bright staining confined to the cell membrane (scale bar = 26.5 µm) (n = 11-13 islets from 4 mice). **B) LUXendin492, LUXendin551** and **LUXendin615** signal can still be detected following formalin-fixation, and is co-localized with orthogonal emission from a specific monoclonal antibody against GLP1R (mAb) (scale bar = 85 µm) (n = 9-10 islets from 4 mice).

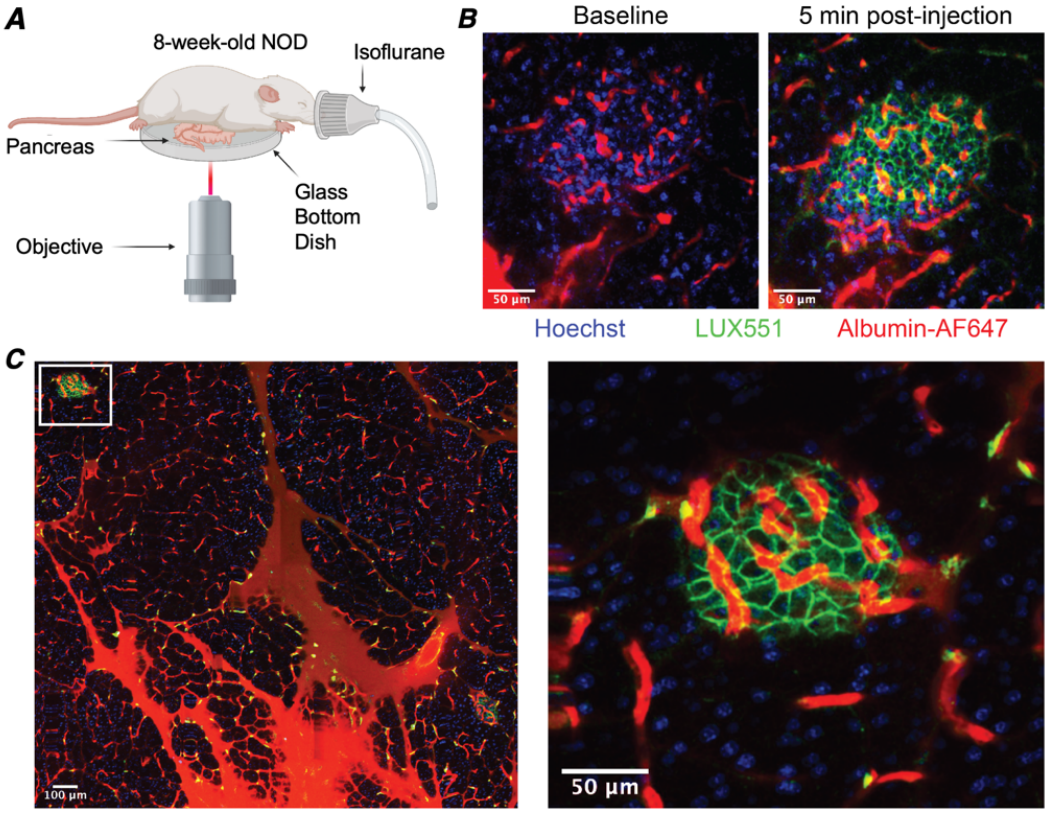

Figure 4: Labelling of GLP1R in NOD mouse islets *in vivo.* A) Two-photon intravital imaging schematic for visualization of the exposed intact pancreas in an 8-week-old NOD mouse. **B)** Representative image collected at baseline and 5 min post-injection showing islet vasculature and accumulation of **LUXendin551** at cell membranes (scale bar = 50 µm). **C)** Mosaic image of externalized pancreas (scale bar = 100 µm) and enlarged islet within this region (scale bar = 50 µm).

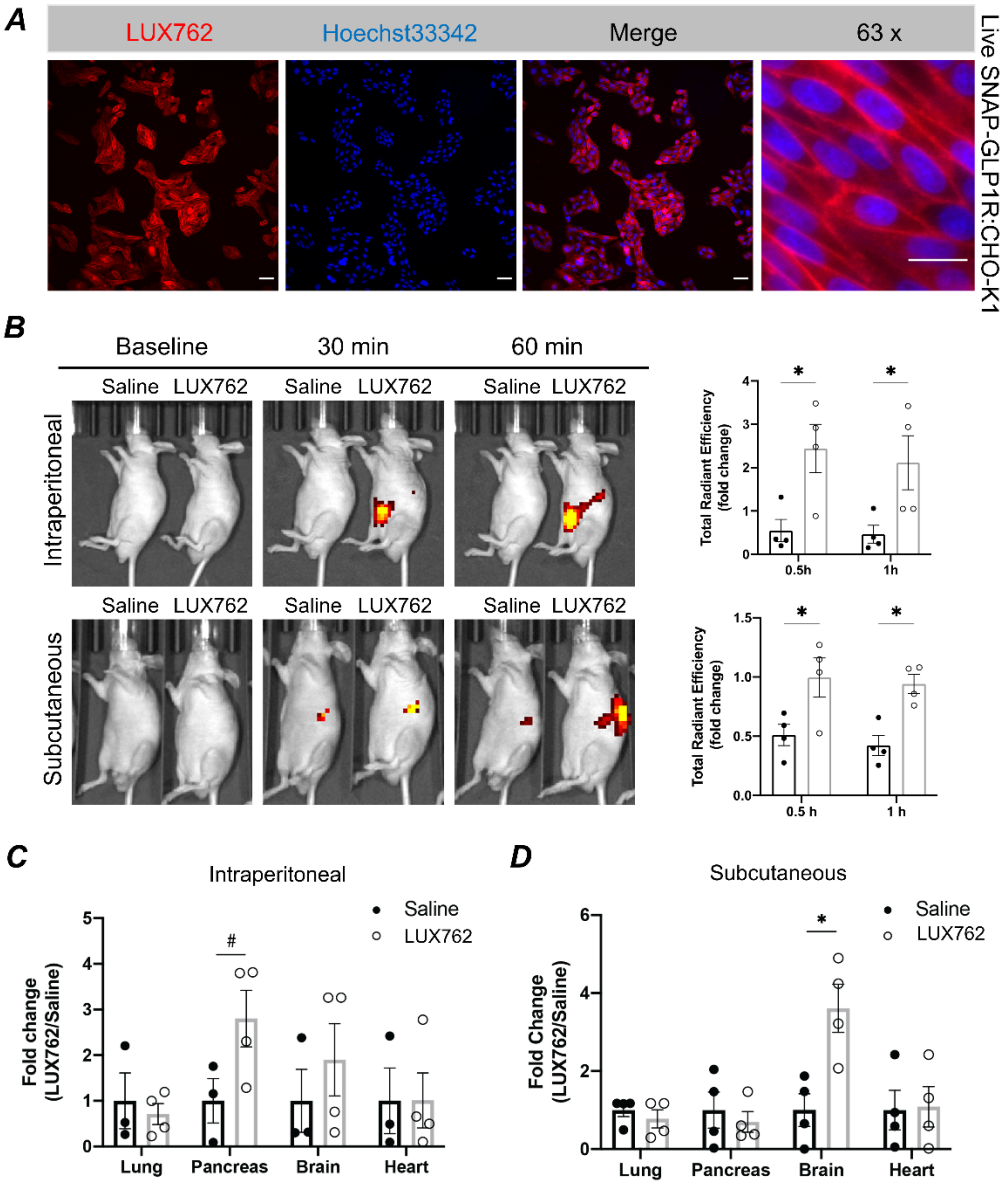

Figure 5: Evaluation of LUXendin762 distribution *in vivo*. A) LUXendin762 (LUX762, 200 nM) labels the membrane of SNAP-GLP1R:CHO-K1 cells (nuclei were stained using Hoechst33342) (scale bar = 50 µm) (n = 3 independent experiments). **B)** *In vivo* images of mice intraperitoneally- or subcutaneously-injected with saline or **LUXendin762** at baseline, 30 mins and 1 hour post injection. Data plotted as fold change of total radiant efficiency signals of whole body measured at 30 minutes and 1 hour post injection. **C)** *Ex vivo* analysis of harvested tissues 1h post intraperitoneal injection (n = 4 mice). **D)** *Ex vivo* analysis of tissues 1 hour post subcutaneous injection (n = 4 mice). Graphs show mean ± SEM. #p=0.08, *p<0.05 (unpaired t test for each tissue).

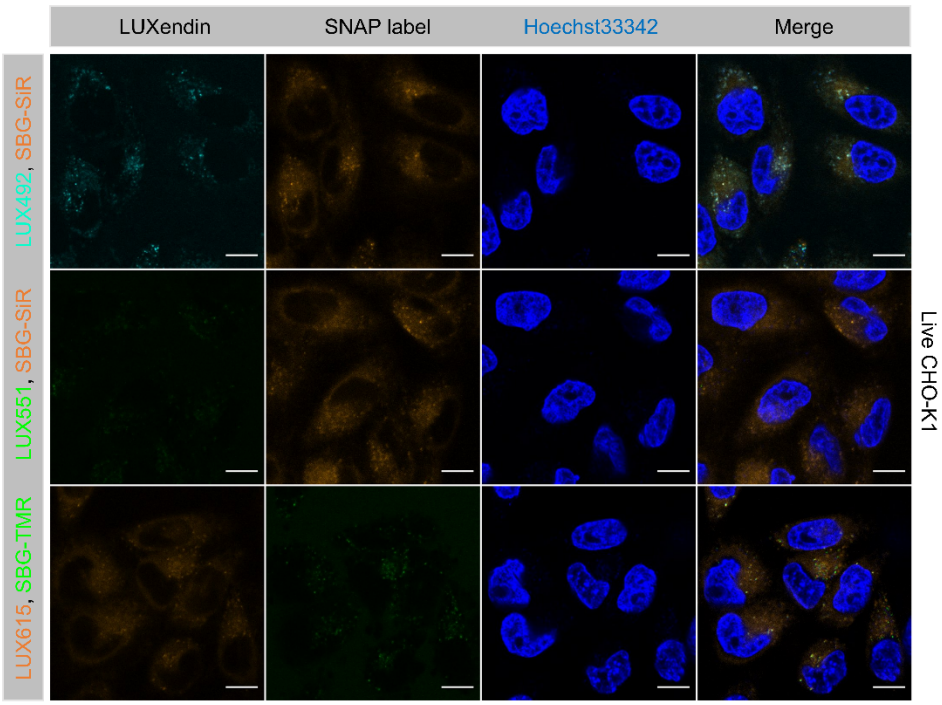

Supplementary Figure 1: Labeling of live CHO-K1 cells with LUXendin492, LUXendin551 and LUXendin615. CHO-K1 cells were treated with **LUXendin492** (LUX492), **LUXendin551** (LUX551) and **LUXendin615** (LUX615), the same way and at the same time as SNAP-GLP1R:CHO-K1 in Figure 2 (scale bar = 10 µm).

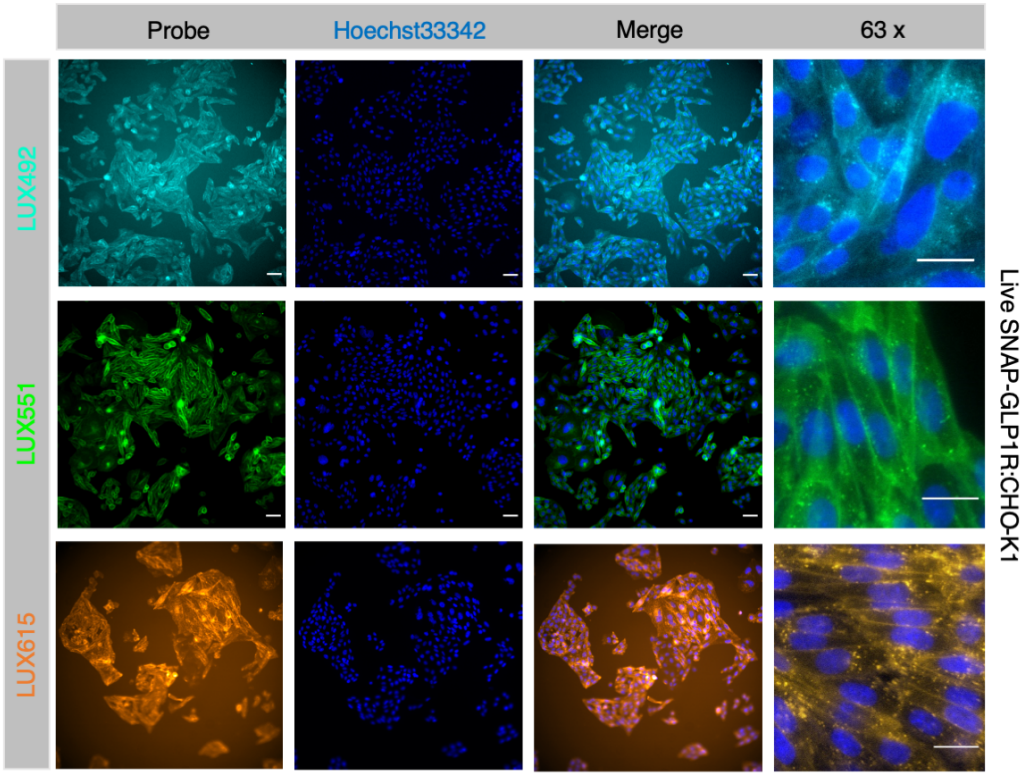

555

556 **Supplementary Figure 2**: **Widefield imaging of LUXendin492, LUXendin551 and**
557 **LUXendin615** labelling. SNAP-GLP1R:CHO-K1 were labelled with **LUXendin492** (LUX492),
558 **LUXendin551** (LUX551) and **LUXendin615** (LUX615), before widefield imaging (scale bar =
559 50 µm) (n = 3 independent experiments). Nuclei were stained using Hoechst33342.

560
561

562

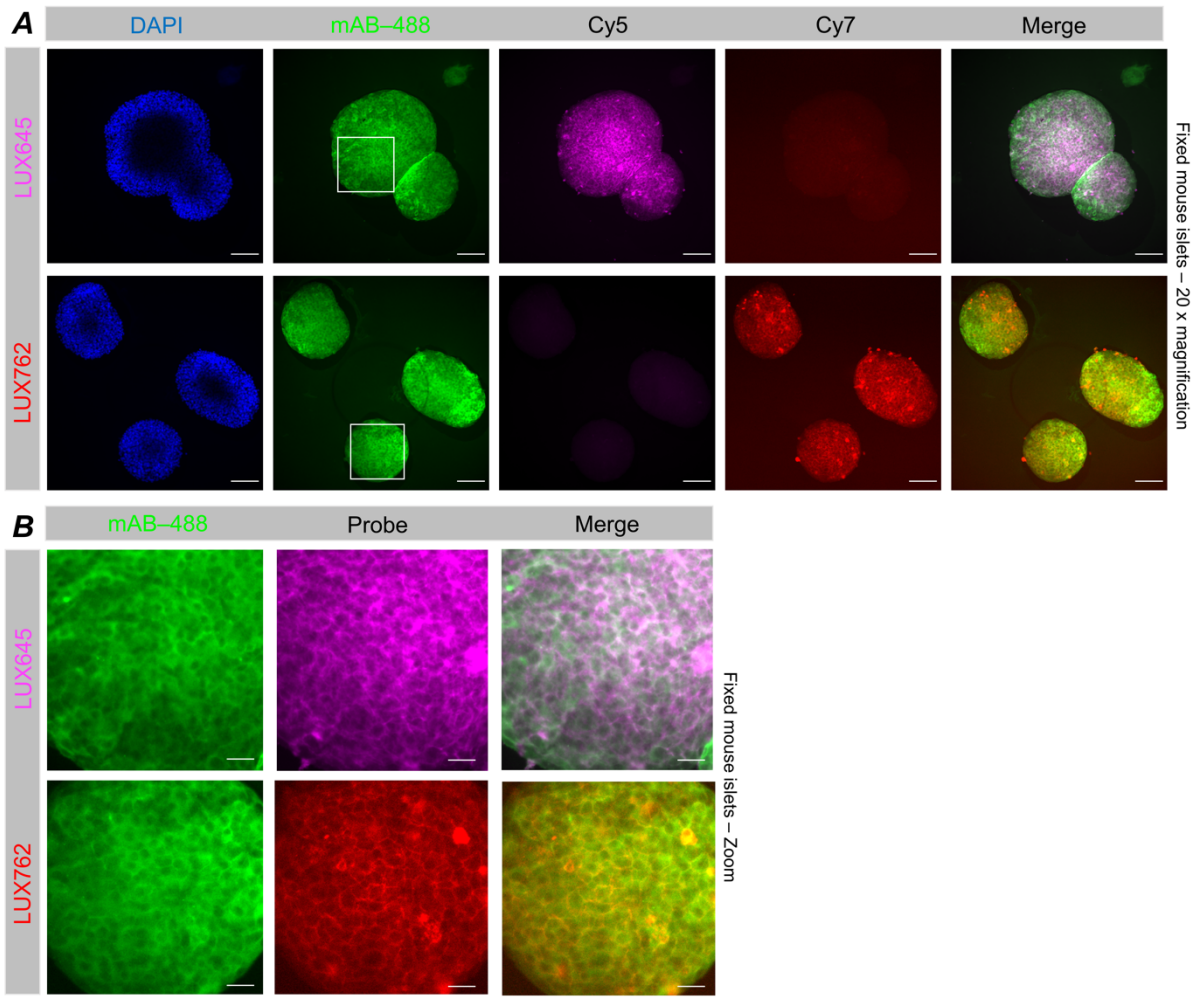

563

564 **Supplementary Figure 3: Labelling of fixed islets of Langerhans with LUXendin762. A)**
565 Islets labelled with **LUXendin762** (LUX762) can be formaldehyde fixed, allowing co-staining
566 with GLP1R monoclonal antibody (mAb-488). **LUXendin645** (LUX645) was used as a known
567 positive control (scale bar = 100 µm) (n > 5 islets from 3 animals). **B)** Zoom-in from **A**) showing
568 overlap between **LUXendin762**/mAb-488 and **LUXendin645**/mAb-488 (scale bar = 25 µm) (n
569 > 5 islets from four animals).

570